Two Bulky-Decorated Triangular Dysprosium Aggregates Conserving Vortex-Spin Structure

Shufang Xue,[†,‡] Xiao-Hua Chen,[§] Lang Zhao,[†] Yun-Nan Guo,[†,‡] and Jinkui Tang*,[†]

[†]State Key Laboratory of Rare Earth Resource Utilization, Changchun Institute of Applied Chemistry, Chinese Academy of Sciences, Changchun 130022, People's Republic of China

[‡]University of Chinese Academy of Sciences, Beijing 100039, People's Republic of China

[§]College of Materials Science and Engineering, Fujian Normal University, Fuzhou 350007, People's Republic of China

Ⓢ *Supporting Information*

ABSTRACT: The self-assembly of dysprosium(III) with the tailored chemical modification of the vanillin group affords two decorated Dy_3 compounds, namely, $[Dy_3(\mu_3\text{-}OH)_2(Hpovh^-)_3(NO_3)_3(CH_3OH)_2\text{-}H_2O]\cdot NO_3\cdot 3CH_3OH\cdot 2H_2O$ (**2**) and $[Dy_3(\mu_3\text{-}OH)_2(H_2vovh^-)_3Cl_2(CH_3\text{-}OH)(H_2O)_3][Dy_3(\mu_3\text{-}OH)_2(H_2vovh^-)_3Cl_2(H_2O)_4]\cdot Cl_4\cdot 2CH_3OH\cdot 2CH_3\text{-}CN\cdot 7H_2O$ (**3**), where H_2povh = *N*-(pyridylmethylene)-*o*-vanilloylhydrazone and H_3vovh = *N*-vanillidene-*o*-vanilloylhydrazone. Of particular interest is that those two title Dy_3 compounds maintain the peculiar vortex-spin structure of the ground nonmagnetic doublet. Complex **2** displays frequency-dependent slow magnetic relaxation, while **3** still inherits the single-molecule-magnet behavior as the parent Dy_3 prototype. The dissimilar dynamic magnetic behavior originates from the structural differences in light of the coordination environment of Dy^{III} ions, which influence the local tensor of anisotropy and crystal-field splitting on each Dy site.
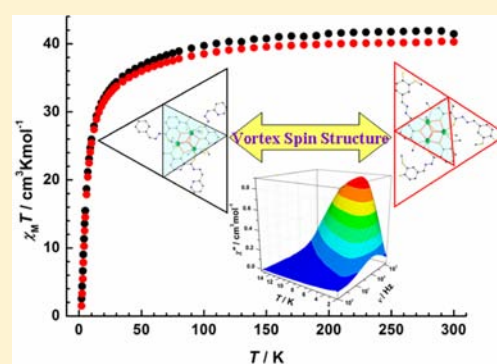
INTRODUCTION

As the archetype of noncollinear spin systems, vortex-spin chirality in the triangular Dy_3 cluster $[Dy_3(\mu_3\text{-}OH)_2L_3Cl\text{-}(H_2O)_5]Cl_3$ (**1**) (where L is the anion of *o*-vanillin) presents a new concept for magnetic memory with no net magnetic moment.[1] This unwonted behavior results from the toroidal arrangement of the local magnetization vector along Dy^{III} ions, as revealed by single-crystal magnetic studies[2] and muon spin–lattice relaxation measurements,[3] as well as corroborated by ab initio calculations.[4,5] Since then, successive efforts have concentrated on the exploitation of magnetically interesting Dy_3 building blocks to create larger dysprosium(III) single-molecule magnets (SMMs);[6−13] thereinto, a unique Dy_6 SMM by the dimerization of two Dy_3 triangular prototypes exhibits spectacular enhancement of the slow magnetic relaxation temperature from the original 8 to 25 K.[7]

Recent efforts have also been engaged in the design of ligands to stabilize the dysprosium cluster with triangular topology.[14−19] However, these tailor-made slow-relaxing Dy_3 triangles do not display the characteristic spin chirality of the local spin, which render us to wonder what kinds of ligands or ligand fields do promote this fascinating spin structure. It is likely to operate via a buildup approach to modify the *o*-vanillin ligands, which favor the trapping of Dy_3 triangles and incorporate other groups to steer the structural and spin features within a triangle system. Herein, we have grafted bulky hydrazine onto the vanillin group (Scheme 1). Such linear ligands provide basic chelating sites as the *o*-vanillin group that

Scheme 1. Structural Representation of the Ligands
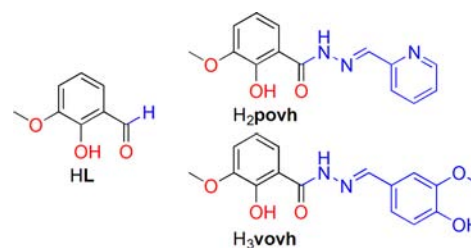
are especially preferable to manufacturing of the targeted configuration. The assembly of proposed ligands with dysprosium(III) nitrate or chloride in MeOH/CH_3CN leads to two decorated Dy_3 compounds, namely, $[Dy_3(\mu_3\text{-}OH)_2\text{-}(Hpovh^-)_3(NO_3)_3(CH_3OH)_2H_2O]\cdot NO_3\cdot 3CH_3OH\cdot 2H_2O$ (**2**) and $[Dy_3(\mu_3\text{-}OH)_2(H_2vovh^-)_3Cl_2(CH_3OH)(H_2O)_3][Dy_3(\mu_3\text{-}OH)_2(H_2vovh^-)_3Cl_2(H_2O)_4]\cdot Cl_4\cdot 2CH_3OH\cdot 2CH_3CN\cdot 7H_2O$ (**3**), where H_2povh = *N*-(pyridylmethylene)-*o*-vanilloylhydrazone and H_3vovh = *N*-vanillidene-*o*-vanilloylhydrazone (see the Experimental Section). Of particular interest is that those two title Dy_3 compounds maintain the peculiar vortex-spin structure of the ground nonmagnetic doublet as the parent type. The dissimilar dynamic magnetic behavior originates from the structural differences in light of the coordination environment
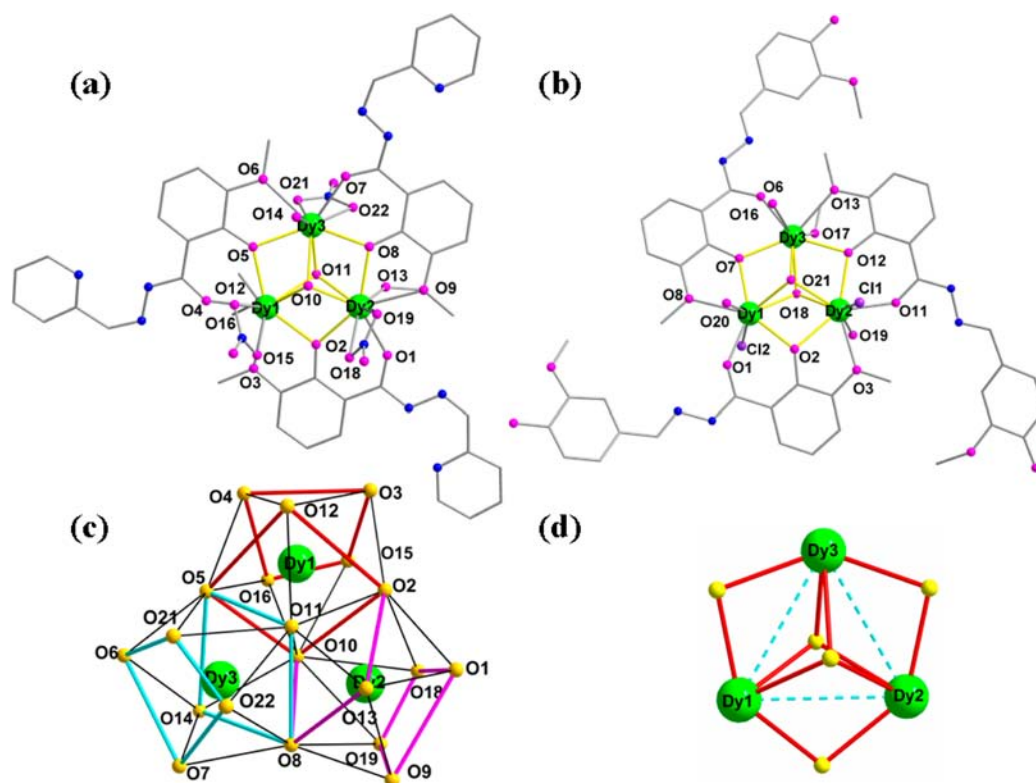
Figure 1. Partially labeled Dy$_3$ structures of complexes **2** (a) and **3** (b) with H atoms omitted for clarity. Color scheme: green, Dy; pink, O; blue, N; purple, Cl. (c) Coordination polyhedra observed in **2**: a monocapped square-antiprismatic environment for Dy. (d) Overall central core for **1−3**.

of Dy^{III} ions, which influence the local tensor of anisotropy and crystal-field splitting on each Dy site.

■ EXPERIMENTAL SECTION

General Procedures. All chemicals were used as commercially obtained without further purification. Elemental analysis for carbon, hydrogen, and nitrogen were carried out on a Perkin-Elmer 2400 analyzer. Fourier transform infrared (FTIR) spectra were recorded with a Perkin-Elmer FTIR spectrophotometer using the reflectance technique (4000−300 cm^{-1}). Samples were prepared as KBr disks. All magnetization data were recorded on a Quantum Design MPMS-XL7 SQUID magnetometer. The variable-temperature magnetization was measured with an external magnetic field of 1000 Oe in the temperature range of 1.9−300 K. Samples were restrained in eicosane to prevent torquing. The experimental magnetic susceptibility data are corrected for the diamagnetism estimated from Pascal's tables[20] and sample holder calibration.

X-ray Crystallography. Suitable single crystals with dimensions of 0.25 × 0.21 × 0.18 and 0.25 × 0.23 × 0.19 mm^3 for **2** and **3**, respectively, were selected for single-crystal X-ray diffraction analysis. Crystallographic data were collected at a temperature of 191 K on a Bruker Apex II CCD diffractometer with graphite-monochromated Mo Kα radiation (λ = 0.71073 Å). Data processing was accomplished with the *SAINT* processing program. The structure was solved by direct methods and refined on F^2 by full-matrix least squares using *SHELXTL97*.[21] The location of the Dy atom was easily determined, and the O, N, and C atoms were subsequently determined from difference Fourier maps. The non-H atoms were refined anisotropically. The H atoms were introduced in calculated positions and refined with fixed geometry with respect to their carrier atoms. In complex **3**, the DFIX command has been used to refine the distances of C−C and C−O in the vanillin group to be in the reasonable range. The FLAT command has been used to refine the C and O atoms from the vanillin group to be in one plane. Isotropic treatment has been done with the solvent molecules. CCDC 890979 (**2**) and 890980 (**3**) contain the supplementary crystallographic data for this paper (see the Supporting

Information). These data can also be obtained free of charge from the Cambridge Crystallographic Data Centre via www.ccdc.cam.ac.uk/data_request/cif.

Synthesis of the Ligands. The ligands H$_2$povh and H$_3$vovh were prepared in a simple hydrazone condensation reaction of *o*-vanilloylhydrazine with picolinaldehyde and vanillin in methanol, respectively. Then the mixture was stirred overnight with the formation of a white suspended solid. The fine white precipitate was filtered off and washed with methanol. For H$_2$povh, the crude product was obtained as a white powder in 60% yield. Anal. Calcd (found) for C$_{14}$H$_{13}$N$_3$O$_3$: C, 61.99 (61.41); H, 4.83 (4.75); N, 15.49 (13.35). IR (KBr, cm^{-1}): 3560(w), 3502(m), 3228(w), 3077(w), 2966(w), 2936(w), 1630(s), 1600(s), 1584(s), 1559(s), 1491(s), 1465(s), 1442(m), 1426(m), 1377(w), 1361(s), 1333(w), 1296(s), 1256(s), 1183(m), 1173(m), 1138(w), 1105(w), 1083(m), 1048(m), 1007(m), 952(m), 915(w), 895(w), 835(m), 796(m), 782(m), 709(w), 671(w), 629(w), 592(m), 457(w). For H$_3$vovh, the crude product was obtained as a white powder in 75% yield. Anal. Calcd (found) for C$_{16}$H$_{16}$N$_2$O$_5$: C, 60.75 (60.18); H, 5.10 (5.04); N, 8.86 (8.79). IR (KBr, cm^{-1}): 3608(w), 3262(br), 2942(w), 2842(w), 1645(s), 1602(s), 1578(s), 1555(s), 1512(s), 1479(s), 1430(s), 1379(w), 1346(w), 1301(s), 1272(s), 1244(s), 1219(m), 1195(m), 1168(m), 1125(w), 1091(w), 1068(m), 1028(m), 972(m), 932(m), 868(w), 811(w), 802(w), 759(w), 748(w), 693(w), 628(m), 530(w), 422(w).

Synthesis of [Dy$_3$(μ_3-OH)$_2$(Hpovh$^-$)$_3$(NO$_3$)$_3$(CH$_3$OH)$_2$H$_2$O]·NO$_3$·3CH$_3$OH·2H$_2$O (2). A suspension of Dy(NO$_3$)$_3$·6H$_2$O (0.2 mmol, 91.2 mg) and H$_2$povh (0.2 mmol, 54.2 mg) in CH$_3$OH/CH$_3$CN (10 mL/10 mL) was treated with NaHCO$_3$ (0.4 mmol, 33.6 mg). The ensuing orange solution was stirred for 6 h and subsequently filtered. The filtrate was left undisturbed to allow the slow evaporation of the solvent. Yellow plate-shaped single crystals of **2**, suitable for X-ray diffraction analysis, formed after 1 week. Yield: 38 mg (25%, based on the metal salt). Anal. Calcd (found) for C$_{47}$H$_{64}$N$_{13}$O$_{31}$Dy$_3$: C, 31.45 (31.26); H, 3.59 (3.51); N, 10.15 (10.09). IR (KBr, cm^{-1}): 3523(br), 3231(br), 3056(w), 3025(w), 2851(w), 1639(s), 1613(s), 1600(w), 1551(s), 1475(s), 1443(m), 1410(w), 1384(s), 1320(m),

1285(s), 1244(w), 1210(w), 1152(w), 1068(w), 1001(w), 966(w), 890(m), 862(w), 798(w), 763(m), 690(m), 664(w), 623(w), 516(w).

Synthesis of [Dy$_3$(μ_3-OH)$_2$(H$_2$vovh$^-$)$_3$Cl$_2$(CH$_3$OH)(H$_2$O)$_3$]- [Dy$_3$(μ_3-OH)$_2$(H$_2$vovh$^-$)$_3$Cl$_2$(H$_2$O)$_4$]·Cl$_4$·2CH$_3$OH·2CH$_3$CN·7H$_2$O (3). A suspension of DyCl$_3$·6H$_2$O (0.2 mmol, 75.4 mg) and H$_3$vovh (0.2 mmol, 63.2 mg) in CH$_3$OH/CH$_3$CN (5 mL/10 mL) was treated with Et$_3$N (0.3 mmol, 42 μL). The ensuing orange solution was stirred for 6 h and subsequently filtered. The filtrate was left undisturbed to allow the slow evaporation of the solvent. Light-yellow block-shaped single crystals of **3**, suitable for X-ray diffraction analysis, formed after 3 days. Yield: 38 mg (25%, based on the metal salt). Anal. Calcd (found) for C$_{103}$H$_{140}$N$_{14}$O$_{51}$Cl$_8$Dy$_6$: C, 33.90 (33.76); H, 3.86 (3.78); N, 5.37 (5.32). IR (KBr, cm^{-1}): 3523(br), 3231(br), 3056(w), 3025(w), 2851(w), 1639(s), 1613(s), 1600(w), 1551(s), 1475(s), 1443(m), 1410(w), 1384(s), 1320(m), 1285(s), 1244(w), 1210(w), 1152(w), 1068(w), 1001(w), 966(w), 890(m), 862(w), 798(w), 763(m), 690(m), 664(w), 623(w), 516(w).

■ RESULTS AND DISCUSSION

Crystal Structures of 2. The reaction of Dy(NO$_3$)$_3$·6H$_2$O with H$_2$povh in methanol/acetonitrile in the presence of NaHCO$_3$ produces yellow crystals of **2** after 1 week. Single-crystal X-ray studies reveal that **2** crystallizes in the monoclinic space group C2/c. A perspective view of the molecular structure of **2** is represented in Figure 1a. Details for the structure solution and refinement are summarized in Table 1, and

Table 1. Crystallographic Data and Structure Refinement for Complexes 2 and 3

	2	3
formula	C$_{47}$H$_{64}$N$_{13}$O$_{31}$Dy$_3$	C$_{103}$H$_{140}$N$_{14}$O$_{51}$Cl$_8$Dy$_6$
M_r	1794.61	3648.89
color	yellow block	colorless block
cryst syst	monoclinic	hexagonal
space group	C2/c	P6$_5$
T [K]	191(2)	191(2)
a [Å]	44.3182(15)	22.759(3)
b [Å]	14.3574(5)	22.759(3)
c [Å]	22.1404(8)	25.477(5)
α [deg]	90	90
β [deg]	108.0420(10)	90
γ [deg]	90	120
V [Å^3]	13395.1(8)	11428(3)
Z	8	3
ρ_{calcd} [g cm^{-3}]	1.780	1.591
F(000)	7064	5388
R$_{int}$	0.0402	0.0491
R1 [I > 2σ(I)]	0.0387	0.0443
wR2 (all data)	0.1209	0.1459
GOF	1.050	1.077

selected bond distances and angles are listed in Table 2. Complex **2** has a similar two-μ_3-OH-capped triangular skeleton, as observed in **1**, in which the vertices of the triangles are linked via bridging phenol O (O2, O5, and O8) atoms of three Hpovh$^-$ ligands with an average Dy–O–Dy angle of 97.894°. For the sake of brevity, we only highlight the differences of the remaining coordination sites around the metallic centers: for **2**, there is a terminal nitrate ion on each metal site, and the required coordinated sites have been fulfilled with solvent molecules. Accordingly, each nine-coordinate Dy^{III} ion in **2** possesses a slightly distorted monocapped square-antiprismatic geometry with O$_9$ coordination sites (Figure 1c). As shown in Figures 2 and S1 in the Supporting Information, the packing of

the structure along different directions for **2** is quite different from that of the parent compound. Further, there are intermolecular long hydrogen-bonding chains between pairs of triangular units by virtue of the nitrate ions and capping hydroxide/solvent molecules. The shortest Dy···Dy distance between adjacent molecules is 9.725 Å.

Crystal Structures of 3. The reaction of DyCl$_3$·6H$_2$O with H$_3$vovh in methanol/acetonitrile, in the presence of Et$_3$N, produces yellow crystals of **3**, which crystallizes in the hexagonal space group P6$_5$, and the representation of the triangular Dy^{III} cluster is depicted in Figure 1b. In **3**, the [Dy$_3$(μ_3-OH)$_2$]$^{7+}$ unit is surrounded with three deprotonated H$_2$vovh$^-$ ligands, each of which connects two Dy^{III} ions with the 2.1$_1$2$_{12}$3$_2$ bridging mode indicated by Harris notation.[22] It is worth noting that in **3** the decoration of the o-vanillin group with the bulky fraction has little effect on the coordination of the Dy^{III} ion. All eight-coordinate Dy^{III} centers thus still possess the original pentagonal bipyramid as the parent complex **1** with one missing site in the pentagonal plane, which can be defined as phenolate oxygen (O2 and O7), carbonyl O1, and methoxy O8 in the case of Dy1. The required coordinated pockets for Dy1 and Dy2 are completed by one Cl ion and one water molecule on the two opposite sides of the plane, while for Dy3, the same sites are occupied by a water molecule above the plane and below a methanol or a water molecule with a 50:50 disorder. When attention is diverted to the metal core, it is easily reminiscent of the parent type because both title compounds are also uninodal, with the vertex symbol of each node being (3) (Figure 1d).[23] The crystal packing of complex **3** in different directions is represented in Figures 3 and S2 in the Supporting Information, and the projection along the [001] direction shows a snowflaked pattern.

Magnetic Properties. Direct-current (dc) magnetic susceptibility measurements of **2** and **3** show the corresponding $\chi_M T$ product values at room temperature of 41.45 and 40.28 cm^3 K mol^{-1} (Figure 4), which indicate that the Stark sublevels of the $^6H_{15/2}$ ground state split by the ligand field are statistically populated at room temperature and the free-ion approximation applies.[24] The corresponding χT value represents a monotonic decrease upon lowering of the temperature up to zero at 1.9 K for **2** and **3**, indicative of the almost nonmagnetic ground state like in other reported lanthanide-based clusters with a toroidal magnetic moment.[1,7,25] The low-temperature behavior is broadly similar to that of the parent Dy$_3$ cluster with a maximum of around 6.5 K under an external field of 1 kOe (Figure 4, inset).

Magnetization (M) data for **2** and **3** were collected in the 0–70 kOe field range below 5 K. The magnetization rises abruptly at low fields before leveling to 14.6 μ_B for **2** (16.9 μ_B for **3**) around 20 kOe at 1.9 K. Those values approximately correspond to the expected value (3 × 5.23 μ_B) for three isolated Dy^{III} ions because of the considerable crystal-field effects.[26] The non-superimposition of the M versus H/T data on a single master curve (Figure 5) suggests the presence of magnetic anisotropy and/or the lack of a well-defined ground state, indicating the presence of low-lying excited states that might be populated when a field is applied.

Despite the fact that the vortex-spin structures were conserved in both complexes **2** and **3** based on the criterion of the vanishing susceptibility for a system comprising an odd number of centers with a half-integer J value, they perform a distinct behavior of magnetic dynamics revealed by alternating-current (ac) susceptibility under zero field. As shown in Figure

Table 2. Selected Bond Distances (Å) and Angles (deg) in Complexes 2 and 3

			Compound **2**				
Dy1–O2	2.360(4)	Dy1–O3	2.543(5)	Dy1–O4	2.286(4)	Dy1–O5	2.327(4)
Dy1–O10	2.312(4)	Dy1–O11	2.381(4)	Dy1–O(2	2.410(5)	Dy1–O15	2.441(6)
Dy1–O16	2.634(6)	Dy2–O1	2.256(5)	Dy2–O2	2.328(4)	Dy2–O8	2.332(4)
Dy2–O9	2.493(5)	Dy2–O10	2.312(4)	Dy2–O11	2.389(4)	Dy2–O13	2.437(5)
Dy2–O18	2.509(6)	Dy2–O19	2.520(6)	Dy3–O5	2.358(4)	Dy3–O6	2.497(5)
Dy3–O7	2.315(4)	Dy3–O8	2.333(4)	Dy3–O10	2.444(4)	Dy3–O11	2.295(4)
Dy3–O14	2.403(5)	Dy3–O21	2.468(6)	Dy3–O22	2.581(6)	Dy1–Dy2	3.5210(4)
Dy1–Dy3	3.5480(4)	Dy2–Dy3	3.5166(4)				
Dy1–O2–Dy2	97.35(16)	Dy1–O10–Dy2	98.68(16)	Dy1–O11–Dy2	95.14(15)		
Dy1–O5–Dy3	98.45(16)	Dy1–O10–Dy3	95.97(16)	Dy1–O11–Dy3	98.70(16)		
Dy2–O8–Dy3	97.85(15)	Dy2–O10–Dy3	95.33(16)	Dy2–O11–Dy3	97.30(16)		
			Compound **3**				
Dy1–O1	2.275(6)	Dy1–O2	2.304(6)	Dy1–O7	2.349(6)	Dy1–O8	2.484(6)
Dy1–O18	2.358(6)	Dy1–O20	2.372(8)	Dy1–O21	2.387(6)	Dy1–Cl2	2.716(3)
Dy2–O2	2.330(6)	Dy2–O3	2.462(6)	Dy2–O11	2.271(6)	Dy2–O12	2.315(7)
Dy2–O18	2.374(6)	Dy2–O19	2.414(8)	Dy2–O21	2.348(6)	Dy2–Cl1	2.712(3)
Dy3–O6	2.265(7)	Dy3–O7	2.298(6)	Dy3–O12	2.320(7)	Dy3–O13	2.462(7)
Dy3–O16	2.364(8)	Dy3–O17	2.369(8)	Dy3–O18	2.374(6)	Dy3–O21	2.358(6)
Dy1–Dy2	3.5322(8)	Dy1–Dy3	3.5259(7)	Dy2–Dy3	3.5139(8)		
Dy1–O2–Dy2	99.3(2)	Dy1–O18–Dy2	96.6(2)	Dy1–O21–Dy2	96.5(2)		
Dy1–O7–Dy3	98.7(2)	Dy1–O18–Dy3	96.4(2)	Dy1–O21–Dy3	96.0(2)		
Dy2–O12–Dy3	98.6(3)	Dy2–O18–Dy3	95.5(2)	Dy2–O21–Dy3	96.6(2)		
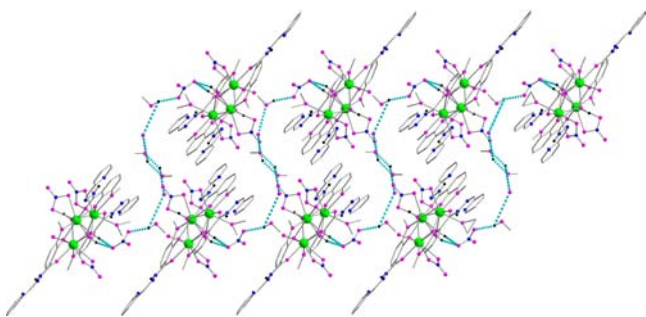
Figure 2. Illustration showing the hydrogen-bonding interactions along the [010] direction of pairs of triangular units in **2**.

6, the low-temperature ac susceptibility for **2** displays frequency-dependent signals characteristic of slow magnetic relaxation. However, the out-of-phase signal (χ'') accounts for only a small component of the total ac susceptibility. As previously observed for many lanthanide systems,[27−31] the ratio of the intensities of the out-of-phase (χ'') and in-phase (χ') signals is far away from the ideal 1:1 at T_{max} of χ''. We emphasize that the series of χ'' peaks around 5 K cannot simply be attributed to the blocking of the anisotropy barrier but are an instinctive response by the sudden fall of the susceptibility (χ_M in Figure 4) as the temperature decreases. Additionally, the absence of frequency-dependent peaks in χ'' signals (Figure S3 in the Supporting Information) may be caused by the presence of a relatively fast zero-field relaxation. Thus, ac data have also been recorded under a small dc field in order to suppress a possible fast zero-field quantum. Upon application of 1 kOe, a strong frequency dependence of ac susceptibility with varying temperature was observed (Figure S4 in the Supporting Information). The relaxation times extracted by the generalized Debye model[32] were fitted by using the Orbach thermally activated relaxation law. The Arrhenius plot shows a crossover
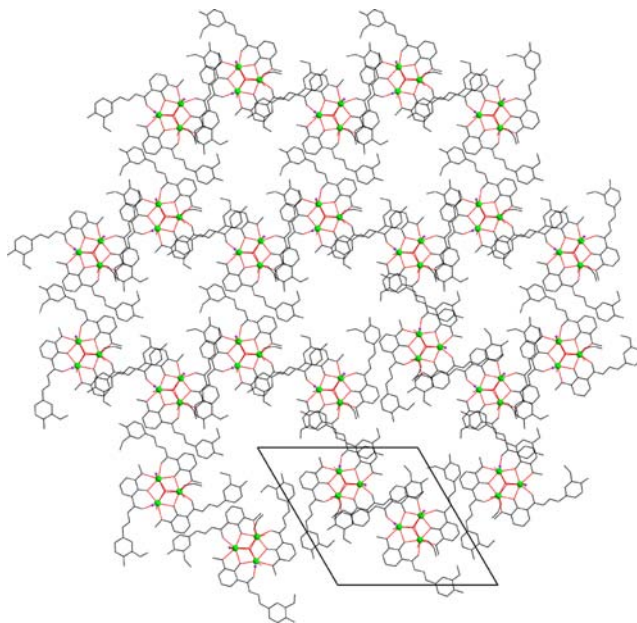
Figure 3. Perspective view down the [001] direction highlighting the channels in **3** (solvent molecules, counterions, and H atoms are omitted for clarity).

at around $T^{-1} = 0.12$ K^{-1}, which suggests the presence of dual relaxation pathways (Figure S5 in the Supporting Information). Linear data corresponding to the law were obtained for the low- and high-temperature domains (solid line, Figure S6 in the Supporting Information), with effective energy barriers of $U_{eff} = 6.0(1)$ and $53.8(7)$ K and preexponential factors of $\tau_0 = 9.5(2) \times 10^{-5}$ and $2.4(2) \times 10^{-7}$, respectively. This is probably attributed to the single-ion behavior of individual Dy^{III} ions at higher temperatures, while the weak coupling with neighboring Dy^{III} ions might become important at low temperatures.[33]
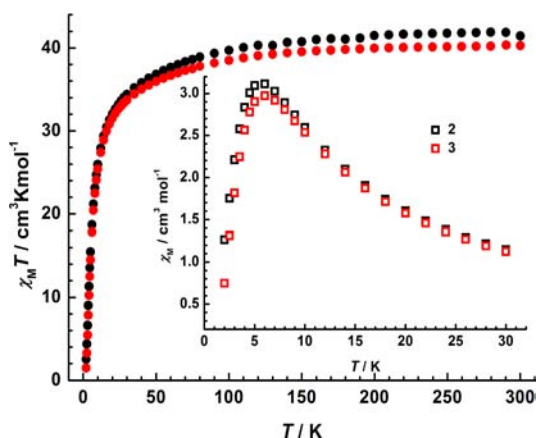
Figure 4. Temperature dependence of the χT product for **2** and **3**. Inset: low-temperature susceptibility χ_M.
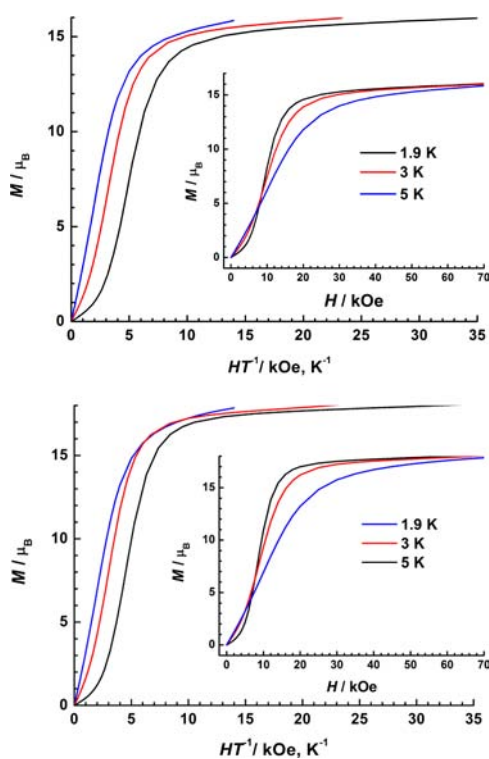
Figure 5. Plots of the reduced magnetization M versus H/T in the field range 0−35 kOe and temperature range 1.9−5.0 K. Insets: Field dependences of magnetization (top) for **2** and (bottom) for **3**.

Figure 6. Temperature-dependent ac susceptibility data for **2** collected under a zero dc field at the indicated frequency.
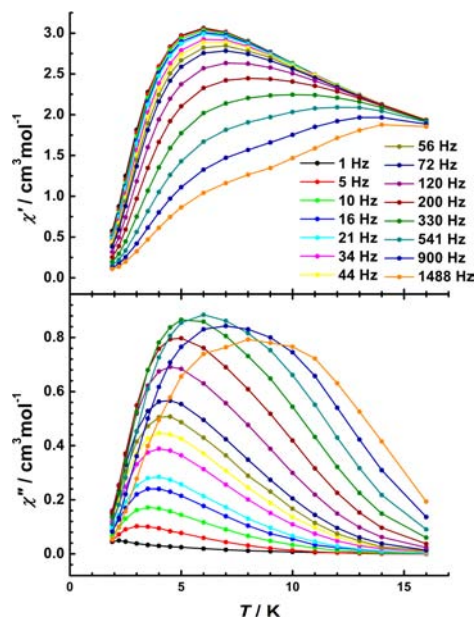
Figure 7. Temperature-dependent ac susceptibility data for **3** collected under a zero dc field at the indicated frequency.

On the contrary, for **3**, χ'' shows a maximum value around 10 K for 1500 Hz (Figure 7), which is higher than the temperature corresponding to the maximum of the dc susceptibility (Figure 4, inset). Meanwhile, the shift of χ'' peaks exhibits a strong frequency dependence as the temperature decreases, which is clearly suggestive of slow relaxation of the magnetization associated with the SMM behavior. Interestingly, complex **3** almost inherits the characteristics of magnetic dynamics in the parent **1**, as shown in Figures 7 and S6 and S7 in the Supporting Information, that the peaks in the frequency-dependent ac susceptibility are quite distorted with a shoulder structure.[1] To quantify its slow relaxation, the relaxation time was extracted from the frequency-dependent data between 1.9 and 16 K and Arrhenius plots were constructed to investigate the temperature-dependent magnetic relaxation (Figure 8). On

the basis of the data above 8 K, the relaxation time exhibits an exponential dependence on the temperature, and an Arrhenius fit $[\tau = \tau_0 \exp(U_{eff}/kT)]$ to the data gives an effective relaxation barrier (U_{eff}) of 21.7(2) K with a preexponential factor (τ_0) of $1.3(1) \times 10^{-5}$ s for **3**. At lower temperatures ($T < 8$ K), the dynamics of **3** become weakly temperature-dependent, indicating the onset of quantum tunneling, which is responsible for the absence of the M versus H hysteresis loop at 1.9 K (Figure S8 in the Supporting Information). Cole−Cole plots with quasisemicircle shape were obtained (Figure S9 in the Supporting Information). Fitting the data by the generalized Debye function[32,34] gives high values of α ($\alpha < 0.32$) in the
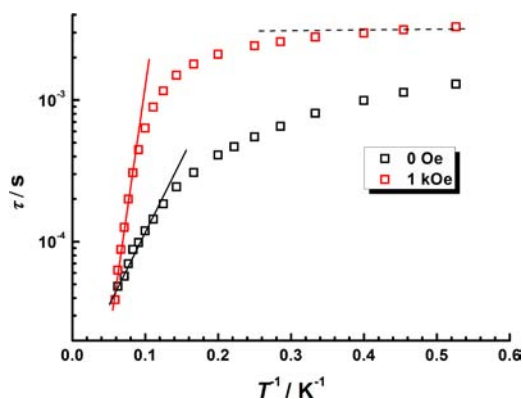
Figure 8. Magnetization relaxation time, τ, versus T^{-1} plot for **3** under 0 and 1 kOe dc field. The solid line is fitted with the Arrhenius law. Error bars are not shown because they lie within the radius of the symbols.

temperature range of 1.9−12 K, suggestive of a wide distribution of relaxation time constants.

Because of the strong field dependence on the dynamics of the magnetization for the parent compound, field dependence studies have also been performed on **3**. Indeed, such a type of behavior also occurs for **3** because the H_{dc} field dependence of χ'' at 7 K reveals that the relaxation time, corresponding to the maximum of χ'', dramatically increases up to the saturating point around 5 kOe and then decreases as the field is applied (Figures 9 and 10). Thus, a second minimum is observed
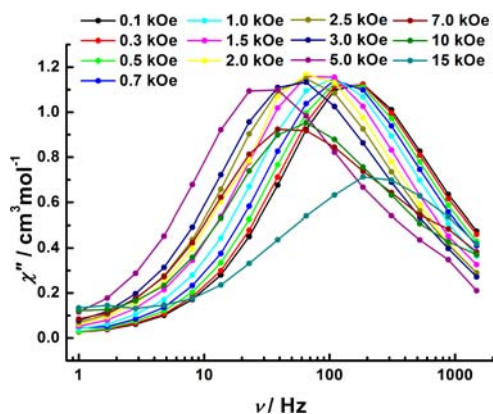
Figure 9. Out-of-phase ac susceptibility (χ'') collected on **3** at 7 K under the indicated dc field.
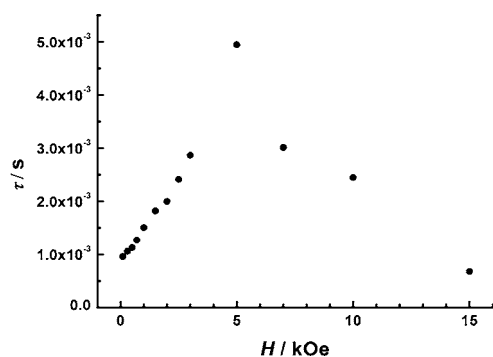
Figure 10. Field dependence of the relaxation time measured at T = 7 K.

around slightly higher field (15 kOe), the field at which corresponds to the first level crossover by the Zeeman effect (Figure 10). This may be indicative of the stronger intramolecular interaction observed in **3** than the parent compound because the position of the minimum is directly related to the magnitude of magnetic interaction. In order to obtain quantitative information regarding the spin-relaxation barrier of **3**, the frequency dependence of χ'' at fixed temperatures under 1 kOe applied field was examined, indicating that relatively higher-temperature relaxation occurs in **3** (Figure 11).
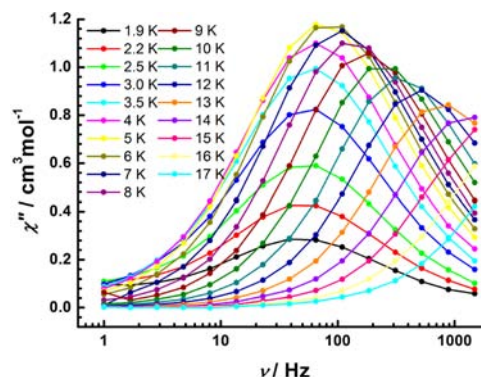
Figure 11. Frequency dependence of χ'' of **3** under an applied dc field of 1 kOe.

The results demonstrate that, for **3**, the relaxation time is significantly increased in the temperature range 1.9−4 K (Figure 8), in which the quantum relaxation process is effective. On the other hand, the Arrhenius fitting between 12 and 17 K (solid line, Figure 8) gives a strongly enhanced barrier of U_{eff} = 82.2(3) K, with τ_0 = 3.4(1) × 10^{-7} s. This thermal behavior resembles that of the parent compound: far from the zero field and level crossing field, it seems to occur through an Orbach process involving the first excited Kramers doublet of each of the Dy^{3+} ions.[2] The ab initio calculations are thus planned in order to provide more precise information on the Ising model to shed light on the spin chirality.

Although compounds **2** and **3** retain similar static magnetic behavior, the dynamic mechanism is drastically different. Indeed, for **2**, χ'' only accounts for a small component of the total susceptibility under zero field, while **3** maintains the slow relaxation of magnetization as the parent type. These distinctive magnetic behaviors must be caused by subtle but crucial structural differences between the respective structures. Actually, a closer look at the two structures reveals important disparities.

As is evidenced in Figure 1 and Table 2, the individual Dy sites in **2** are nine-coordinate, derived from two phenoxide O, one carbonyl O, one methoxide group, two μ_3-OH ligands, one terminal nitrate ion in η^2 fashion, and solvent molecules. The Dy−O−Dy angles through μ_3-OH range from 95.14(15) to 98.70(16)°; the Dy−O−Dy angles between adjacent Dy^{III} ions through μ-O$^-$ fall in the range of 97.35(16)−98.45(16)°. The skeleton of **3** is essentially isomorphous to **2**, with the terminal nitrate in **2** having been replaced by Cl ions (for Dy1 and Dy2) or a solvent molecule (for Dy3); thus, all eight-coordinate Dy^{III} centers thus still possess the original pentagonal bipyramid as the parent type. In contrast to **2**, the Dy−O−Dy angles through μ_3-OH lie between 95.5(2) and 96.6(2)°; the Dy−O−Dy angle between adjacent Dy ions through μ-O$^-$ is well above 98.6°.

The main, significant disparities between the two triangular dysprosium aggregates are thus found in the coordination environment of Dy^{III} ions. The distinctive relaxation dynamics of lanthanide compounds mainly results from the large intrinsic magnetic anisotropy of the metal ions, which is governed both by the chemical environment of the metal center and occupation of the relevant f orbitals. These structural differences clearly affect the local tensor of anisotropy and crystal-field splitting on each Dy site, therefore generating dissimilar dynamic magnetic behavior.[35−37]

CONCLUSION

We reported two decorated Dy$_3$ triangular compounds with tailored chemical modification of the vanillin group. The feature lies in the fact that (1) both of them maintain the original vortex-spin structure as the parent compound and (2) the significant magnetic disparities of the title compounds may be associated with the distinct anisotropic centers mainly because of the direct influence of the different ligand field. Therefore, the synthetic strategy illustrated in this work represents a promising buildup approach to designing ligands that favor the trapping of Dy$_3$ triangles with specific noncollinear spin nature and incorporating other ligating groups into these ligands in order to influence the electronic properties of the molecule to construct multifunctional materials.

ASSOCIATED CONTENT

Ⓢ Supporting Information

X-ray crystallographic data in CIF format, crystal packing of complexes **2** and **3**, ac susceptibility data, frequency dependence, magnetization relaxation data, field dependence of magnetization, and Cole−Cole plots. This material is available free of charge via the Internet at http://pubs.acs.org.

AUTHOR INFORMATION

Corresponding Author
*E-mail: tang@ciac.jl.cn.

Notes

The authors declare no competing financial interest.

ACKNOWLEDGMENTS

REFERENCES

(1) Tang, J.; Hewitt, I.; Madhu, N. T.; Chastanet, G.; Wernsdorfer, W.; Anson, C. E.; Benelli, C.; Sessoli, R.; Powell, A. K. *Angew. Chem., Int. Ed.* **2006**, *45*, 1729−1733.
(2) Luzon, J.; Bernot, K.; Hewitt, I. J.; Anson, C. E.; Powell, A. K.; Sessoli, R. *Phys. Rev. Lett.* **2008**, *100*, 247205.
(3) Salman, Z.; Giblin, S. R.; Lan, Y.; Powell, A. K.; Scheuermann, R.; Tingle, R.; Sessoli, R. *Phys. Rev. B* **2010**, *82*, 174427.
(4) Chibotaru, L. F.; Ungur, L.; Soncini, A. *Angew. Chem., Int. Ed.* **2008**, *47*, 4126−4129.
(5) Ungur, L.; Heuvel, W. V. d.; Chibotaru, L. F. *New J. Chem.* **2009**, *33*, 1224−1230.
(6) Hussain, B.; Savard, D.; Burchell, T. J.; Wernsdorfer, W.; Murugesu, M. *Chem. Commun.* **2009**, 1100−1102.
(7) Hewitt, I. J.; Tang, J.; Madhu, N. T.; Anson, C. E.; Lan, Y.; Luzon, J.; Etienne, M.; Sessoli, R.; Powell, A. K. *Angew. Chem., Int. Ed.* **2010**, *49*, 6352−6356.
(8) Tian, H.; Guo, Y.-N.; Zhao, L.; Tang, J.; Liu, Z. *Inorg. Chem.* **2011**, *50*, 8688−8690.
(9) Ke, H.; Zhao, L.; Guo, Y.; Tang, J. *Eur. J. Inorg. Chem.* **2011**, *2011*, 4153−4156.
(10) Ke, H.; Xu, G.-F.; Zhao, L.; Tang, J.; Zhang, X. Y.; Zhang, H. J. *Chem.—Eur. J.* **2009**, *15*, 10335−10338.
(11) Zhao, L.; Xue, S.; Tang, J. *Inorg. Chem.* **2012**, *51*, 5994−5996.
(12) Novitchi, G.; Pilet, G.; Ungur, L.; Moshchalkov, V. V.; Wernsdorfer, W.; Chibotaru, L. F.; Luneau, D.; Powell, A. K. *Chem. Sci.* **2012**, *3*, 1169−1176.
(13) Guo, F.-S.; Guo, P.-H.; Meng, Z.-S.; Tong, M.-L. *Polyhedron* **2011**, *30*, 3079−3082.
(14) Hewitt, I. J.; Lan, Y.; Anson, C. E.; Luzon, J.; Sessoli, R.; Powell, A. K. *Chem. Commun.* **2009**, 6765−6767.
(15) Liu, C.-S.; Du, M.; Sanudo, E. C.; Echeverria, J.; Hu, M.; Zhang, Q.; Zhou, L.-M.; Fang, S.-M. *Dalton Trans.* **2011**, *40*, 9366−9369.
(16) Guo, F.-S.; Liu, J.-L.; Leng, J.-D.; Meng, Z.-S.; Lin, Z.-J.; Tong, M.-L.; Gao, S.; Ungur, L.; Chibotaru, L. F. *Chem.—Eur. J.* **2011**, *17*, 2458−2466.
(17) Anwar, M. U.; Tandon, S. S.; Dawe, L. N.; Habib, F.; Murugesu, M.; Thompson, L. K. *Inorg. Chem.* **2012**, *51*, 1028−1034.
(18) Lin, S.-Y.; Zhao, L.; Guo, Y.-N.; Zhang, P.; Guo, Y.; Tang, J. *Inorg. Chem.* **2012**, *51*, 10522−10528.
(19) Lin, S.-Y.; Guo, Y.-N.; Guo, Y.; Zhao, L.; Zhang, P.; Ke, H.; Tang, J. *Chem. Commun.* **2012**, *48*, 6924−6926.
(20) Boudreaux, E. A.; Mulay, L. N. *Theory and Applications of Molecular Paramagnetism*; John Wiley & Sons: New York, 1976.
(21) Sheldrick, G. M. *SHELXS-97, Program for Crystal Structure Solution*; University of Göttingen: Göttingen, Germany, 1997.
(22) Coxall, R. A.; Harris, S. G.; Henderson, D. K.; Parsons, S.; Tasker, P. A.; Winpenny, R. E. P. *J. Chem. Soc., Dalton Trans.* **2000**, 2349−2356.
(23) Kostakis, G. E.; Powell, A. K. *Coord. Chem. Rev.* **2009**, *253*, 2686−2697.
(24) Kahn, O. *Molecular Magnetism*; Wiley-VCH: New York, 1993.
(25) Guo, P.-H.; Liu, J.-L.; Zhang, Z.-M.; Ungur, L.; Chibotaru, L. F.; Leng, J.-D.; Guo, F.-S.; Tong, M.-L. *Inorg. Chem.* **2012**, *51*, 1233−1235.
(26) Xu, G. F.; Wang, Q. L.; Gamez, P.; Ma, Y.; Clérac, R.; Tang, J. K.; Yan, S. P.; Cheng, P.; Liao, D. Z. *Chem. Commun.* **2010**, *46*, 1506−1508.
(27) Ishikawa, N.; Sugita, M.; Ishikawa, T.; Koshihara, S.-y.; Kaizu, Y. *J. Am. Chem. Soc.* **2003**, *125*, 8694−8695.
(28) Lin, P. H.; Burchell, T. J.; Clérac, R.; Murugesu, M. *Angew. Chem., Int. Ed.* **2008**, *47*, 8848−8851.
(29) Feltham, H. L. C.; Lan, Y.; Klöwer, F.; Ungur, L.; Chibotaru, L. F.; Powell, A. K.; Brooker, S. *Chem.—Eur. J.* **2011**, *17*, 4362−4365.
(30) Guo, Y.-N.; Chen, X.-H.; Xue, S.; Tang, J. *Inorg. Chem.* **2012**, *51*, 4035−4042.
(31) Xue, S.; Zhao, L.; Guo, Y.-N.; Tang, J. *Dalton Trans.* **2012**, *41*, 351−353.
(32) Aubin, S. M. J.; Sun, Z.; Pardi, L.; Krzystek, J.; Folting, K.; Brunel, L.-C.; Rheingold, A. L.; Christou, G.; Hendrickson, D. N. *Inorg. Chem.* **1999**, *38*, 5329−5340.
(33) Sharples, J. W.; Zheng, Y.-Z.; Tuna, F.; McInnes, E. J. L.; Collison, D. *Chem. Commun.* **2011**, *47*, 7650−7652.
(34) Cole, K. S.; Cole, R. H. *J. Chem. Phys.* **1941**, *9*, 341−351.
(35) Norel, L.; Bernot, K.; Feng, M.; Roisnel, T.; Caneschi, A.; Sessoli, R.; Rigaut, S. *Chem. Commun.* **2012**, *48*, 3948−3950.
(36) Rinehart, J. D.; Long, J. R. *Chem. Sci.* **2011**, *2*, 2078−2085.
(37) Lin, P. H.; Burchell, T. J.; Ungur, L.; Chibotaru, L. F.; Wernsdorfer, W.; Murugesu, M. *Angew. Chem., Int. Ed.* **2009**, *48*, 9489−9492.